





Cascade Latent Heat Storage for Solar Cooking Applications

Shubham Jain¹ , K. Ravi Kumar^{1,*} , Dibakar Rakshit¹ ,
B. Premachandran² , and K. S. Reddy³ 

¹ Department of Energy Science and Engineering, Indian Institute of Technology Delhi, India

² Department of Mechanical Engineering, Indian Institute of Technology Delhi, India

³ Department of Mechanical Engineering, Indian Institute of Technology Madras, India

*Correspondance: K. Ravi Kumar, krk@dese.iitd.ac.in

Abstract. The present investigation explores the potential of multiple phase change material (PCM) based storage for real-time solar thermal applications. There are two types of storage configurations tested in this work for the simultaneous charging and discharging operation, i.e., single PCM-based NaNO₃ storage and 2-stage cascade latent heat storage having NaNO₃ and NaNO₂ as the storage mediums in the consecutive stages. The storage is designed to achieve the end-use temperature condition of 513 K (the highest temperature required for cooking) with the latent thermal energy accumulation capacity of 1 MJ. The study envisages that instead of using a single PCM in the storage unit, 2-stage cascading of the PCMs can improve energy accumulation and retrieval in storage. After 8 hours of operation, none of the storage achieves the complete charging state. The energy accumulated in the NaNO₃/NaNO₂ cascade storage is found to be 2.6 times higher than the energy accumulated in the NaNO₃ storage. NaNO₃/NaNO₂ storage achieves the desired constant outlet temperature of cold heat transfer fluid for chapati making (531 K) after 165 minutes of operation. At this moment, the latent energy accumulated in the NaNO₃ and NaNO₃/NaNO₂ storage is observed as 35% and 14%, respectively.

Keywords: Cascade Latent Heat Storage, Phase Change Material, Solar Cooking

1. Introduction

The limited availability of conventional energy sources and their serious impact on the living environment has changed the focus of researchers toward finding clean energy sources for fulfilling the energy needs of society. Nowadays, solar energy, wind energy, geothermal, etc., are some of the potential replacements for conventional energy resources. Low maintenance, scalability modularity, and long-term cost savings are some of the reasons for the wide-scale adoption of solar energy systems. The nocturnal non-availability of solar energy and radiation fluctuations during cloudy weather conditions are major drawbacks that need to be overcome for the growth of solar energy technologies. The use of thermal energy storage in solar energy systems can serve this purpose. Latent heat storage (LHS) is one of the potential options for storing thermal energy received from the sun due to its easy process cycle, low maintenance, easy availability, and low cost [1]. Shell and tube type LHS is one of the most explored configurations of latent thermal storage due to its easy fabrication and low maintenance [2, 3]. Extensive studies are performed on the shell and tube-based LHS to minimize the effect of low

thermal conductivity of the phase change material (PCM) over the charging/discharging behavior of the LHS. These studies include the incorporation of extended metallic structures, heat pipes, nanoparticles in the PCM domain, and macro-micro encapsulation of the PCM in various shapes [4]. The physics involved in melting and solidification is slightly different. Melting is a natural convection-driven process; however, solidification is a conduction-driven process mainly. The curtailment in the charging/discharging rate due to the low thermal conductivity of the medium of the PCM-based LHS can be overcome by incorporating various heat transfer augmentation techniques as per the involved heat transfer mechanism. In a study, Tay et al. [5] have examined pinned and finned storage configurations and observed a 25% better charge cycle performance of finned configuration due to a larger exposed surface area. Robak et al. [6] have observed a 50 % higher melting rate in the LHS having heat pipes compared to the finned LHS. Although Nie et al. [7] underlined a 16% curtailment in the charging time using 0.03% volume of nanoparticles in the PCM domain, the agglomeration issues of nanoparticles limit their applications in PCM-based storages. Another innovative approach to heat transfer augmentation in PCM is the incorporation of a low-density porous structure in the PCM domain. Sardari et al. [8] have tested the storage having a porous matrix. A highly conductive copper foam having variable porosity was inserted in the PCM. It is concluded the charging rate of the copper foam-assisted storage was 85% higher than the storage that does not have copper foam.

For the large-scale acceptability of any method of heat transfer augmentation in latent heat storages (LHS), the method should not have process complexity, and it should be cost-effective. Utilization of multiple PCMs in a single storage unit has both characteristics. Therefore, it is a reliable technology for large-scale applications. The significant decrement in the temperature differential between HTF and PCM in the storage of large size when HTF flows from the inlet toward the outlet negatively affects the thermal energy transfer. It is observed that arranging multiple PCMs in the storage can overcome this negative effect on the performance of the storage [9]. Wang et al. [10] have reported a 37% improvement in the case of using multiple PCM in a latent heat storage unit rather than a single PCM. In another study, Gong and Mujumdar [11] have developed a finite element approach-based model employed to test the five PCM-based cascade latent heat storage (CLHS) having PCMs of melting points 767 °C, 717 °C, 667 °C, 617 °C, and 567 °C. The reported data indicates a 35.1% improvement in the charging rate. In CLHS, the melting/solidification rate depends upon the arrangement of PCMs in the storage unit. Jain et al. [12] have investigated the thermal behavior of the two-stage CLHS having NaNO_3 and NaNO_2 as the PCMs for two different arrangements of the PCMs, i.e., inline and reverse. In the inline arrangement, the PCM has a higher melting temperature placed near the inlet of the heat transfer fluid (HTF), and vice-versa for the reverse arrangement. A total reduction of 30.76% in the melting time was reported using the inline arrangement as compared to the reverse arrangement.

In the existing literature, CLHS has been tested for either charging or discharging applications separately. However, in the context of the practical implementation, the true potential of the CLHS can only be judged based on their behavior during the simultaneous charging and discharging (SCD). In cooking applications, different cooking processes require different operating temperatures [13]. For variable operating temperature demand, CLHS can be a suitable storage configuration to provide energy for end-use applications at different operating temperatures. In this investigation, the true potential of CLHS for variable temperature demand for solar cooking applications is highlighted using the enthalpy porosity-based numerical model.

2. Model Description and Numerical Modelling Procedure

The physical models tested in the study are two 1-stage LHS units having NaNO_3 as PCM and a 2-stage CLHS having two different compartments in a single storage unit. NaNO_3 and NaNO_2 PCMs are filled in Compartment 1 and Compartment 2, respectively. There are two separate

HTF tubes provided in each storage configuration for passing the hot and cold HTF simultaneously (Figure: 1). All three storage configurations have a design capacity of 1 MJ of latent thermal energy. The inner and outer shell diameters are 68.78 mm and 73mm, respectively, while the inner and outer HTF tube diameters are 18.92 mm and 22.22 mm, respectively. Table 1 represents the thermophysical properties of NaNO₃ and NaNO₂ PCMs.

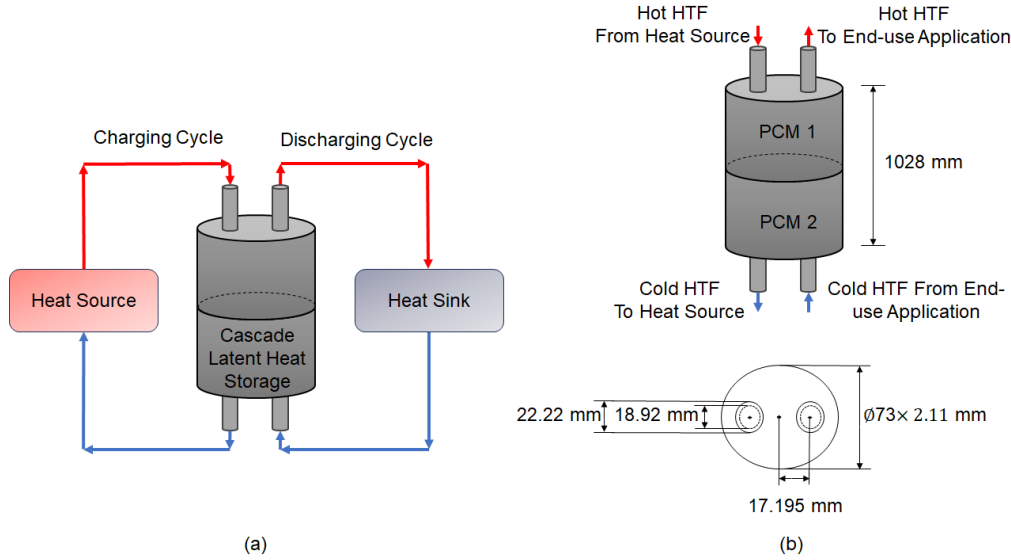


Figure 1. Schematic of the CLHS (a) Operation strategy (b) Description of the CLHS

Table 1. Thermophysical properties of PCMs [1]

Properties	NaNO ₃	NaNO ₂
Melting Temperature (K)	579	555
Enthalpy of Phase Change (kJ/kg)	176	180.12
Coefficient of Thermal Expansion (1/K)	0.0004	0.00028
Specific Heat Capacity (kJ/kg K)	1.60 (solid), 1.655 (liquid)	1.733 (solid), 2.553 (liquid)
Thermal Conductivity (W/m-K)	0.8 (solid), 0.68 (liquid)	0.765 (solid), 0.665 (liquid)
Density (kg/m ³)	1908	1812
Dynamic Viscosity ×10 ⁻⁴ (Pa-s)	26.9	26.66

The present investigations are performed using the enthalpy porosity approach, and simulations are performed using ANSYS 2022R2 [14]. The governing equations solved in the numerical modeling are as follows [1]:

Mass conservation equation [14]:

$$\frac{\partial \rho}{\partial t} + \nabla \cdot (\rho \vec{V}) = 0 \quad (1)$$

Momentum conservation equation [14]:

$$\frac{\partial \rho \vec{V}}{\partial t} + \nabla \cdot (\rho \vec{V} \vec{V}) = -\nabla p + \vec{g} \beta_t \rho_{ref} (T - T_{ref}) + \nabla \cdot (\mu \nabla \vec{V}) - \frac{(1-\beta)^2}{\beta^{3+\varepsilon}} A_{Mushy} \vec{V} \quad (2)$$

Here, A_{Mushy} has a numeric value of 10^5 [15]. The body force term $\vec{g} \beta_t \rho_{ref} (T - T_{ref})$ is included using Boussinesq approximation.

Energy conservation equation [14]:

$$\frac{\partial (\rho H_t)}{\partial t} + \nabla \cdot (\rho \vec{V} H_t) = \nabla \cdot (k \nabla T) \quad (3)$$

Furthermore, the total enthalpy is given as:

$$H_t = h_{ref} + \int_T^{T_m} C_p \partial T + \beta L \quad (4)$$

The melt fraction (β):

$$\beta = \begin{cases} \frac{T - T_{Solidus}}{T_{Liquidus} - T_{Solidus}}; & \text{when } T_{Solidus} < T < T_{Liquidus} \\ 0; & \text{when } T \leq T_{Solidus} \\ 1; & \text{when } T \geq T_{Liquidus} \end{cases} \quad (5)$$

In this study, solid and melted PCMs are homogeneous and isotropic, and no volume change as well as viscous dissipation in PCMs, are considered. Laminar HTF flow with no-slip boundary conditions is modeled here. In the previous study by Jain et al. [12], it was observed that arranging the PCMs in the decreasing order of their melting temperature in the HTF's flow direction in CLHS enhances the charging rate of the storage. In the present work, efforts are made to understand the behavior of the CLHS for the simultaneous charging and discharging operation. A numeric value of 615 K and 519 K are assigned for the entrance temperature of the hot and cold HTF, respectively, by keeping the same difference between the temperature of the HTF and the melting temperature of the PCM in the respective stage at the inlet. Both the HTF flow at a velocity of 0.04 m/s. The PCM domain is initialized at a temperature of 519 K. Based on the grid and time step independence study, 467,857 elements and a time step of 0.1 s are considered in all the simulations performed.

3. Results and Discussion

The observations of the present investigation on CLHS for simultaneous charging and discharging conditions are discussed in the subsequent sections:

3.1 Melting and Solidification Behaviour of Storages

The present study highlights the potential of cascade latent heat storage for solar cooking applications. The storage is tested for SCD condition, in which it receives the energy from the hot HTF and at the same time cold HTF is retrieving the energy from the storage and supplying it to the baking operation. Baking requires the highest temperature (473 K-513 K) compared to the other cooking applications; therefore, in this study, the storage configuration is designed to maintain a cold HTF temperature of 513 K to assist the baking operation. [16]. In the previous study by Jain et al. [9], it was observed that instead of arranging a single PCM in the shell, arrangement of the two PCMs in the shell (CLHS) in the decreasing order of their melting temperature along the HTF's flow directions enhances the charging performance of the storage. In this extended study, two different types of storage are tested for solar cooking applications, and their melting and solidification behavior is evaluated during simultaneous charging and discharging. Two separate HTF flow passages are provided for the hot and cold HTFs, as shown in Figure 1. In one configuration, the NaNO_3 PCM is filled in the shell, while in another,

two different PCMs, such as NaNO_3 and NaNO_2 , are filled in the two consecutive parts of the outer shell. All the storages are investigated for the simultaneous charging and discharging operations, in which the hot HTF enters from the top of the storage and heats the PCM in the surrounding shell. At the same time, cold HTF enters from the bottom of the storage through a separate passage to collect the heat from the storage. All the simulations are performed for 8 hours (average bright sunshine hours in New Delhi) [17]. (The initiation of the melting can be observed after 30 minutes of charging in NaNO_3 storage (Figure 2(a)). However, CLHS shows early initiations of the melting (after 25 minutes). After the initiation of the melting, a faster charging rate is observed in $\text{NaNO}_3/\text{NaNO}_2$ as compared to the NaNO_3 storage due to the higher temperature difference between the hot HTF and the PCMs. The arrangement of the PCM in such a way that the PCM with a higher melting temperature placed near the inlet of the hot HTF and the PCM with a lower melting temperature placed near the inlet of the cold HTF for charging and discharging, respectively offers a uniform thermal energy transfer between the HTF and PCM. This results in a faster energy accumulation in the storage along with the discharging.

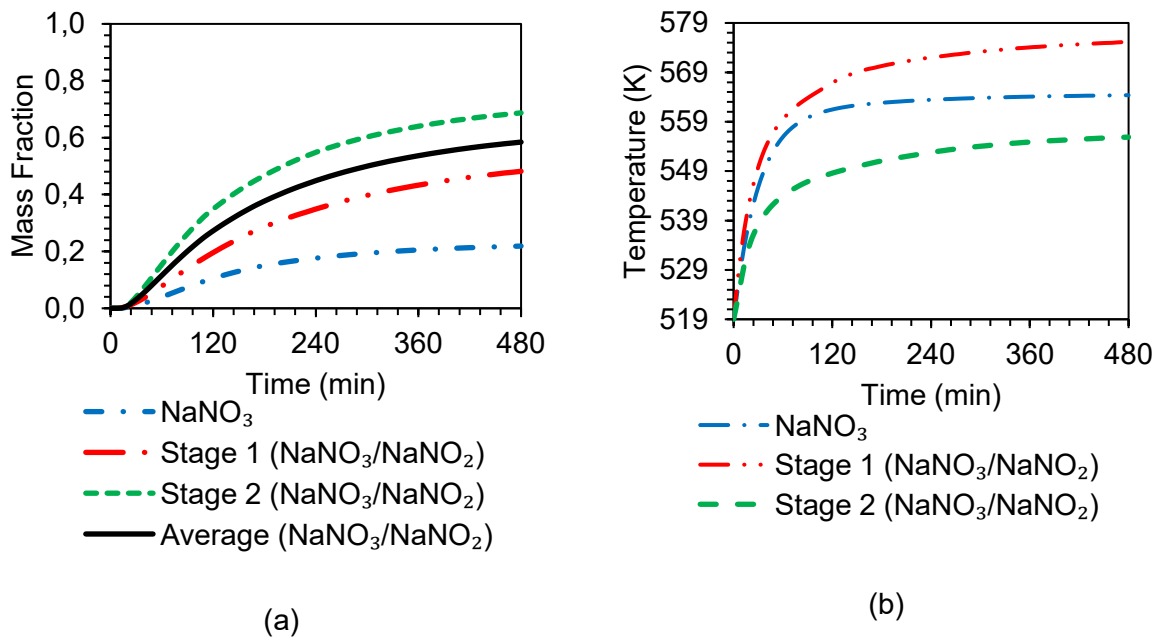


Figure 2. (a) Melt fraction variation and (b) variation of the average temperature of PCMs

The sharp rise during the initial sensible heating phase, followed by reduced temperature variation during the phase change, can be observed in Figure 2(b). In 8 hours of operations, none of the storage has completed the complete melting due to the simultaneous charging and discharging of the storage. After 8 hours of operation, the average melt fraction of the PCMs in CLHS is observed to be 2.6 times higher than the average melt fraction of the NaNO_3 storage. Stage 1 of the CLHS has completed a 48.2% melting; however, stage 2 has completed the 68.7% melting after 8 hours of the operation. The faster rate of melting in stage 2 is due to the better temperature differences between hot HTF and NaNO_2 PCM in stage 2 of the CLHS. The hot HTF transfers the heat to the surrounding shell while passing through the storage, and at the same time, the cold HTF collects the energy from the surrounding shell. As the hot HTF transfers the energy to the PCM near the entrance, a faster melting rate can be observed in Figure 3 compared to the reduced melting rate near the outlet of the hot HTF. The bottom portion of the storage suffers from a reduced melting rate due to the reduced hot HTF temperature and the energy extraction through the cold HTF in this region. The amassment of the melted PCM against gravity also augments the melting in the top part of the storage. The arrangement of the two PCMs in the storage (CLHS) can augment the heat transfer in the bottom part of the storage.

3.2 Energy Stored and End-Use Temperature

The present storage configurations are designed to store the 1 MJ of latent thermal energy. The energy accumulation and retrieval occur at the same time in most of the solar thermal processes, including cooking. Therefore, the designed storage is subjected to real-time boundary conditions to understand the thermal behavior of the storage. Figure 4(a) shows the outlet temperature of the cold HTF in both the storages. After 190 minutes of operation, the cold HTF can provide a constant temperature of 531 K for the end-use application in NaNO_3 storage. The storage is designed to support the chapati-making operation, which requires a temperature of up to 513 K. The designed storage should provide the HTF at a constant temperature higher than 513 K. However, the $\text{NaNO}_3/\text{NaNO}_2$ storage achieves a similar condition earlier than the NaNO_3 storage (after 165 minutes of operation). The $\text{NaNO}_3/\text{NaNO}_2$ storage can maintain a constant temperature condition of up to 533 K for the cold HTF. A significant temperature difference of 20 K can be maintained at the end-use process (cooking).

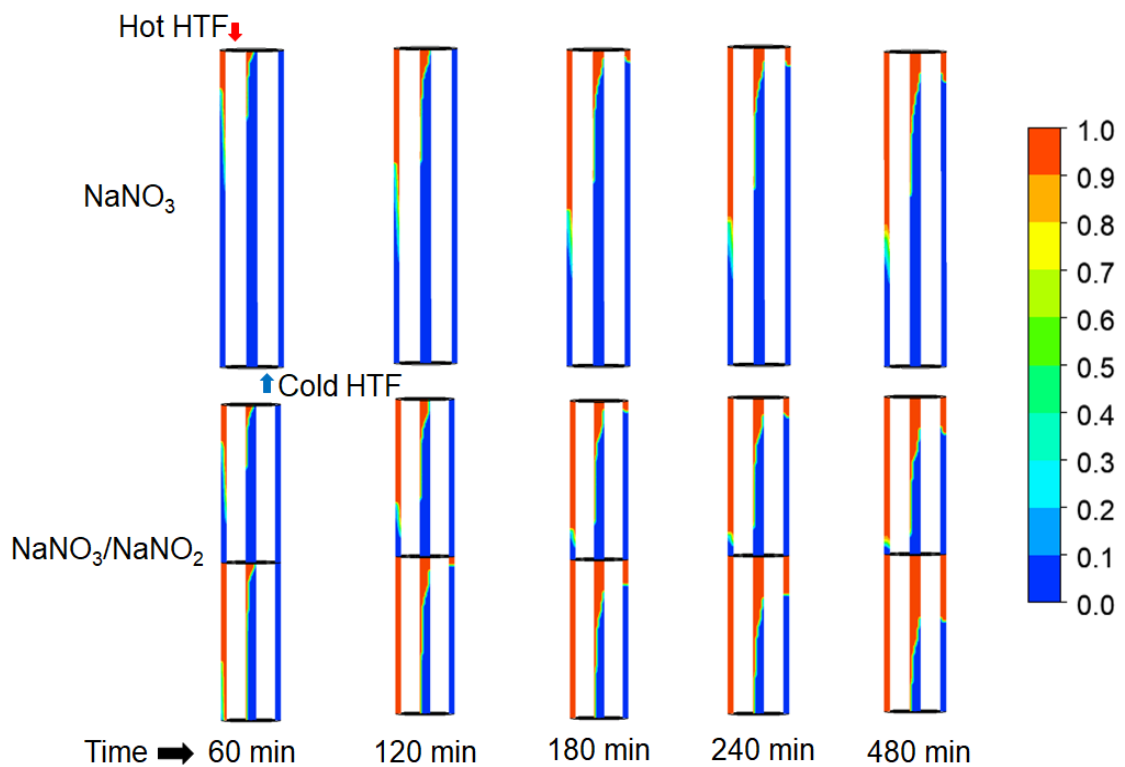


Figure 3. Contours of melt fraction

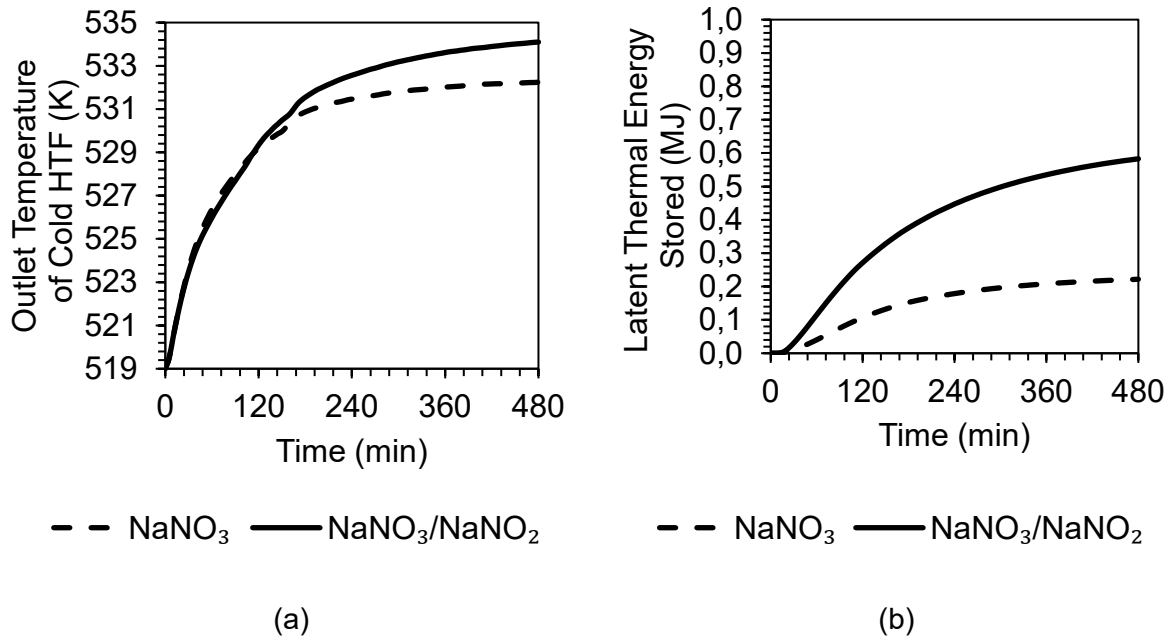


Figure 4. (a) End-use temperature achieved (b) latent energy stored

The true potential of the NaNO₃/NaNO₂ can be highlighted by simultaneously focusing on the energy accumulation in the storage along with the end-use temperature condition. It is evident from Figure 4(a and b) that NaNO₃/NaNO₂ storage can accumulate more latent thermal energy than NaNO₃ storage, along with the required outlet temperature of the cold HTF during discharging. After 8 hours of operation, none of the storage achieves the complete charging state. The energy accumulated in the NaNO₃/NaNO₂ storage is found to be 2.6 times higher than the energy accumulated in the NaNO₃ storage. After 165 minutes of operation, the CLHS achieves 35% of the charging, while NaNO₃ achieves only 14% of the charging. Therefore, the NaNO₃/NaNO₂ storage can support the solar cooking process better than the single PCM-based NaNO₃ storage in terms of the end-use temperature conditions and energy accumulation for simultaneous charging and discharging conditions. Moreover, it can fulfill the need for variable temperature during cooking using PCMs having different melting temperatures in various stages of the CLHS. The aforementioned claim needs further investigation in this context.

4. Conclusions

In the present investigation, the comparative performance evaluation is carried out for the single PCM-based LHS and the CLHS for the simultaneous charging and discharging conditions. It is evident from the results that the slower melting rate at the bottom part of the single PCM-based NaNO₃ storage can be improved using a cascading of two PCMs in the single storage unit. The NaNO₃/NaNO₂ storage can achieve the required outlet conditions earlier than the NaNO₃ storage. The energy accumulated in the NaNO₃/NaNO₂ storage is found to be 2.6 times higher than the energy accumulated in the NaNO₃ storage after 8-hour duration. The NaNO₃/NaNO₂ storage can achieve the required outlet conditions earlier than the NaNO₃ storage. The NaNO₃/NaNO₂ storage stores 58% of the targeted latent thermal energy (1 MJ) after 8 hours of operation. However, the NaNO₃ storage accumulates only 22% of the energy during this period.

Data availability statement

The data that has been used is confidential.

Author contributions

Shubham Jain: Conceptualization, Methodology, Software, Validation, Formal analysis, Data curation, Investigation, Writing original draft, Writing review & editing. Dr. K. Ravi Kumar: Conceptualization, Methodology, Software, Validation, Formal analysis, Data curation, Investigation, Writing original draft, Writing review & editing. Dr. Dibakar Rakshit: Supervision, Writing review & editing. Dr. B. Premachandran: Supervision, Writing review & editing. Dr. K. S. Reddy: Supervision, Writing review & editing.

Competing interests

The authors declare that they have no known competing financial interests or personal relationships that could have appeared to influence the work reported in this paper.

Acknowledgment

The financial support for this research work is provided by the Department of Science and Technology (DST), Government of India, New Delhi, through the research project (Project Number: DST/TMD/CERI/RES/2020/14(G)).

References

- [1] S. Jain, K. R. Kumar, D. Rakshit, B. Premachandran, and K. S. Reddy, "Study on the melting dynamics of latent heat storage for various orientations, shell shapes, and eccentricity," *Thermal Science and Engineering Progress*, vol. 45, no. June, p. 102087, 2023, doi: 10.1016/j.tsep.2023.102087.
- [2] M. E. Zayed, J. Zhao, W. Li, A. H. Elsheikh, A. M. Elbanna, L. Jing, and A. E. Geweda, "Recent progress in phase change materials storage containers: Geometries, design considerations and heat transfer improvement methods," *Journal of Energy Storage*, vol. 30, no. January, p. 101341, 2020, doi: 10.1016/j.est.2020.101341.
- [3] M. J. Li, M. J. Li, X. D. Xue, and D. Li, "Optimization and design criterion of the shell-and-tube thermal energy storage with cascaded PCMs under the constraint of outlet threshold temperature," *Renewable Energy*, vol. 181, pp. 1371–1385, 2022, doi: 10.1016/j.renene.2021.09.086.
- [4] S. Jain, K. R. Kumar, and D. Rakshit, "Heat transfer augmentation in single and multiple (cascade) phase change materials based thermal energy storage: Research progress, challenges, and recommendations," *Sustainable Energy Technologies and Assessments*, vol. 48, no. September, p. 101633, 2021, doi: 10.1016/j.seta.2021.101633.
- [5] N. H. S. Tay, F. Bruno, and M. Belusko, "Comparison of pinned and finned tubes in a phase change thermal energy storage system using CFD," *Applied Energy*, vol. 104, pp. 79–86, 2013, doi: 10.1016/j.apenergy.2012.10.040.
- [6] C. W. Robak, T. L. Bergman, and A. Faghri, "Enhancement of latent heat energy storage using embedded heat pipes," *International Journal of Heat and Mass Transfer*, vol. 54, no. 15–16, pp. 3476–3484, 2011, doi: 10.1016/j.ijheatmasstransfer.2011.03.038.
- [7] C. Nie, J. Liu, and S. Deng, "Effect of geometric parameter and nanoparticles on PCM melting in a vertical shell-tube system," *Applied Thermal Engineering*, vol. 184, no. May 2020, p. 116290, 2021, doi: 10.1016/j.applthermaleng.2020.116290.
- [8] P. T. Sardari, H. I. Mohammed, D. Giddings, G. S. walker, M. Gillott, and D. Grant, "Numerical study of a multiple-segment metal foam-PCM latent heat storage unit: Effect

- of porosity, pore density and location of heat source," *Energy*, vol. 189, p. 116108, 2019, doi: 10.1016/j.energy.2019.116108.
- [9] S. Jain, K. R. Kumar, D. Rakshit, B. Premachandran, and K. S. Reddy, "Influence of the storage orientation and shell shape on the melting dynamics of shell and tube-type cascade latent heat storage," *Applied Thermal Engineering*, vol. 231, no. April, p. 120923, 2023, doi: 10.1016/j.applthermaleng.2023.120923.
- [10] J. Wang, R. Y. Ouyang, and G. Chen, "Experimental study on charging processes of a cylindrical heat storage capsule employing multiple-phase-change materials," *International Journal of Energy Research* vol. 447, no. October 1999, pp. 439–447, 2001, doi: 10.1002/er.695.
- [11] Z. Gong, A. S. Mujumdar "A New Solar Receiver Thermal Store for Space-Based Activities Using Multiple Composite Phase-Change Materials," *J. Sol. Energy Eng.* vol. 1, no. August, pp. 5–10, 1995. <https://doi.org/10.1115/1.2847798>.
- [12] S. Jain, K. R. Kumar, D. Rakshit, B. Premachandran, and K. S. Reddy, "Cyclic performance assessment of medium-temperature cascade thermal energy storage," *Journal of Energy Storage*, vol. 68, no. January, p. 107662, 2023, doi: 10.1016/j.est.2023.107662.
- [13] A. Herez, M. Ramadan, and M. Khaled, "Review on solar cooker systems: Economic and environmental study for different Lebanese scenarios," *Renewable and Sustainable Energy Reviews*, vol. 81, no. February 2017, pp. 421–432, 2018, doi: 10.1016/j.rser.2017.08.021.
- [14] A. D. Brent, V. R. Voller, and K. J. Reid, "Enthalpy-porosity technique for modeling convection-diffusion phase change: Application to the melting of a pure metal," *Numerical Heat Transfer*, vol. 13, no. 3, pp. 297–318, 1988, doi: 10.1080/10407788808913615.
- [15] M. Fadhil and P. C. Eames, "Numerical investigation of the influence of mushy zone parameter $Amush$ on heat transfer characteristics in vertically and horizontally oriented thermal energy storage systems," *Applied Thermal Engineering*, vol. 151, no. January, pp. 90–99, 2019, doi: 10.1016/j.applthermaleng.2019.01.102.
- [16] D. N. Yadav, P. E. Patki, C. Mahesh, G. K. Sharma, and A. S. Bawa, "Optimisation of baking parameters of chapati with respect to vitamin B 1 and B2 retention and quality," *International Journal of Food Science and Technology*, vol. 43, no. 8, pp. 1474–1483, 2008, doi: 10.1111/j.1365-2621.2008.01712.x.
- [17] A. Mani, M. S. Swaminathan, and S. P. Venkiteshwaran, "Distribution of sunshine and solar radiation over the Indian Peninsula", *MAUSAM*, vol. 13, no. 2, pp. 195–212, Apr. 1962. <https://doi.org/10.54302/mausam.v13i2.4338>.